Preparation and Characterization of Novel Mesoporous Ceria−Titania

Anil K. Sinha* and Kenichirou Suzuki

Materials Division, Toyota Central R&D Labs Inc.41-1, Aza, Yokomichi, Nagakute-cho, Aichi-gun, Aichi-ken 480-1192, Japan

Received: August 11, 2004; In Final Form: November 16, 2004

Synthesis of a novel thermally stable mesoporous ceria−titania phase using a neutral templating route is reported. The as-made inorganic-template hybrid mesostructured matrix showed a broad low-angle XRD peak characteristic of mesoporous materials. Careful thermal treatment of the matrix allowed the subsequent densification (of the pore walls) of the inorganic component and removal of the organic component so that a high-quality mesoporous ceria−titania was formed as observed by TEM analysis. The calcined material showed the formation of fluorite type structure of CeO_2 but no crystalline titania phase was observed. The mesoporous structure remained even after high-temperature treatment. The material had high surface area after calcination up to the temperature of 973 K, with well-dispersed ceria and titania components and negligible bulk oxide formation (from XRD, UV−vis, and XPS analysis). These novel mesoporous ceria−titania materials showed high performance for the removal of volatile organic compound (toluene). The toluene removal performance was further enhanced for Pt impregnated mesoporous ceria−titania.

I. Introduction

Ceria-based materials have received enormous attention because of their applications in various fields such as high-temperature ceramics, catalysis, and solid oxide fuel cells.[1] CeO_2 is a well-known additive in the so-called three-way catalysts for automobile exhaust.[2] In particular, supported CeO_2 and CeO_2-based mixed oxides are the effective catalysts for the oxidation of different hydrocarbons and for the removal of organics from polluted water from different sources.[3−6] The incorporation of CeO_2 to the formulation of oxidation catalysts promotes various catalytic reactions such as CO_2 activation,[7] CO oxidation,[3] CO/NO removal,[8] and combustion of hydrocarbons.[9] In all of these applications, two features are mainly responsible for making CeO_2 a promising material for use either as a support or as an active catalyst: (i) the redox couple Ce^{3+}/Ce^{4+}, with the ability of ceria to shift between CeO_2 and Ce_2O_3 under oxidizing and reducing conditions, respectively, and (ii) the ease of formation of labile oxygen vacancies and the relatively high mobility of bulk oxygen species.[10] However, pure ceria is poorly thermostable and undergoes rapid sintering under high-temperature conditions, thereby loosing oxygen buffer capacity.[11,12] Therefore, there have been several attempts to overcome this problem. One approach is the substitution of another metal or metal oxide into the ceria lattice, thereby facilitating the formation of mixed oxides.[13−18] Replacing cerium ions by cations of different size or charge modifies ion mobility inside the modified lattice, resulting in the formation of a defective fluorite-structured solid solution. Such modifications in the defect structure of ceria confer new properties to the catalyst such as better resistance to sintering at high temperatures and high catalytic activity for various reactions.[19] The mixing of two different oxides could result in the formation of new stable compounds that may lead to totally different physicochemical properties and catalytic behavior.[18]

Ceria can be photoactivated by near-UV−vis range irradiation[20] while titania is the most active photocatalyst. These characteristics suggest that ceria−titania mixed oxides could be potentially used as novel photocatalysts, as well as could find application in electrochromic devices.[21] These mixed oxide materials could find application in removal of pollutants such as volatile organic compounds (VOCs). Plastics, paints, varnishes, disinfectants, cosmetics, tobacco smoke, and fuels are some of the household sources of VOCs. Very recently, new photocatalytic filtering systems based on TiO_2 nanoparticles for VOCs decomposition have been installed inside Toyota vehicles for improving air quality.[22] It is highly desirable to develop materials which are more economical, efficient, and convenient to use for room-temperature decomposition/elimination of VOCs materials from in-house and from passenger vehicles.

High surface area nonporous ceria and ceria−zirconia[23] as well as their mesoporous structures[24] have been prepared by different methods, namely, template-assisted method[24] or homogeneous precipitation and microemulsion methods.[23] Such materials by virtue of their large surface area exhibit greater catalytic activity. With the preparation in 1991 of mesoporous silica, a new area of chemistry, allowing the exploitation of high surface area materials, was opened up.[25] The use of surfactants as liquid-crystal templating agents so as to create a regular three-dimensional micellar array about which an inorganic precursor could form a framework gives a reliable method to produce ordered mesoporous solids. The subsequent removal of surfactant in a controlled manner yields a material with an open framework with uniform pore dimensions in the range of 2−10 nm. This silica-based synthesis has been extended to several transition-metal and main group oxides using various surfactants and inorganic precursors under different reaction conditions.[26,27] Herein is reported a neutral templating method employed to form a true mesoporous ceria−titania of uniform pore size with enhanced thermal stability after surfactant removal. Also reported is the detailed characterization of these materials and their potential application as novel indoor VOCs removal material at room temperature.

* Author to whom correspondence should be addressed. Fax: +81−561−63−6137; tel: +81−561−63−7683; e-mail: sinha-anil@mosk.tytlabs.co.jp.

10.1021/jp046391b CCC: $30.25
Published on Web 01/14/2005

II. Experimental Section

Mesoporous ceria−titania with different Ce/Ti ratios (0.5:1, 1:1, 1:1.5) were prepared by a neutral templating route using hexadecylamine as structure-directing reagent and triethanolamine as an additive in mixed propanol−water medium. Role of triethanolamine additive is to act as a complexing agent for the inorganic precursor ions which would result in gradual and homogeneous crystallization of the mixed inorganic oxide phase. In a specific synthesis, hexadecylamine (2.0 g, Wako) was dissolved in propanol (6 g) at 308 K followed by the addition of cerium(III) acetate monohydrate (0.69 g, 99%, Wako) and titanium isopropoxide (0.59 g, 95%, Wako) (for Ce/Ti = 1/1), and the mixture was stirred for 1 h. Then, triethanolamine (0.31 g, 98%, Wako) and water (6.0 g) were added to the gel followed by stirring for 6 h. The final gel was treated at 333 K in a closed vessel for 6 h followed by washing the solid product with ethanol and calcining at 450 °C for 6 h.

Reference mesoporous ceria and mesoporous titania materials were also prepared by a similar reported procedure using hexadecylamine template. Nonporous ceria−titania was also prepared according to a reported procedure.[28] The samples were impregnated with 1 wt % of Pt by incipient-wetness method using aqueous solution of $Pt(NO_3)_2(NH_3)_2$ complex followed by reduction in H_2 atmosphere at 500 °C.

The powder X-ray diffraction (XRD) patterns were obtained on a Rigaku Rint-2400 instrument equipped with a rotating anode and using Cu Kα radiation (wavelength = 0.1542 nm). UV−vis diffuse reflectance spectra were measured at room temperature on a Photal Otsuka Electronics, MC-2530 instrument. Nitrogen adsorption/desorption isotherms were obtained at 77 K on an Autosorb-1 apparatus. Prior to measurement, the samples were heated at 473 K for 2 h and finally outgassed to 10^{-3} Torr. BET and BJH analysis were used to determine the total specific surface area (S_{BET}), pore volume, and pore size distribution of the samples. The Pt dispersion was measured by H_2 chemisorption on a Micromeritics ASAP 2010 instrument at 298 K. The results are expressed as the ratio of the number of moles of hydrogen chemisorbed to the number of moles of Pt in the catalyst. A ratio of 1.00 is defined as 100% dispersion (all the Pt atoms are available for catalysis). Values less than 1.00 may indicate crystallite growth or a surface interference. Particle sizes of Pt dispersed on samples were determined by use of TEM images. Transmission electron microscopy (TEM) observations were made using a JEM200CX instrument. Ti and Ce contents in the catalysts were determined by inductively coupled plasma (ICP) technique.

The XPS measurements were performed on a PHI-5500MC spectrometer by using Mg Kα (1253.6 eV) radiation as the excitation source and with an analysis area of about 800 $\mu m\phi$. Charging of the catalyst samples was corrected by setting the binding energy of the adventitious carbon (C 1s) to 284.6 eV.[30,31] The XPS analysis was done at ambient temperature and pressures typically about 10^{-7} Pa. Prior to analysis, the samples were outgassed in a vacuum oven overnight. The O1s, Ce3d, and Ti2p core-level spectra were recorded.

Mesoporous oxides and Pt impregnated materials were tested for their toluene removal ability at room temperature. As an evaluation gas, a gas mixture was used which contained toluene: 103 ppm, oxygen: 20%, and the balance of nitrogen. Five-tenths gram each of the oxide samples and the evaluation gas (5 L) were put in a 5-L gas container. The gas was analyzed after different time intervals by gas chromatography (Shimadzu GC-12A, FID detector, column SP-1000) and a CO_2 analyzer (LI-6262, LI-COR, Inc.). The toluene removal was determined from the following equation:

$$\text{toluene removal (\%)} = [\{(\text{toluene concentration in gas container without catalyst}) - (\text{toluene concentration in gas container with catalyst})\}/\text{toluene concentration in gas container without catalyst}] \times 100$$

The toluene conversion to CO_2 was determined from the following equation:

$$\text{toluene conversion (\%)} = [\{(CO_2 \text{ concentration in gas container with catalyst}) - (CO_2 \text{ concentration in gas container without catalyst})\}/\text{theoretical } CO_2 \text{ concentration in gas container assuming complete toluene decomposition}] \times 100$$

A packed-bed reactor was used to evaluate catalyst activity in the complete oxidation of toluene (space velocity, 30 000 h^{-1}; toluene, 100 ppm; oxygen, 18%; and the balance of nitrogen). At the onset of the reaction, the catalyst was pretreated with reactant mixture at 180 °C for 1.5 h to prevent overestimation of toluene conversion caused by adsorption of toluene in the initial stages of the test.

TABLE 1: Surface Properties of Mesoporous Ceria−Titania Calcined at Different Temperatures and Those of Reference Materials

oxide samples, temp.	area ($m^2\ g^{-1}$)	pore size (nm)	pore volume (ccg^{-1})	Ce:Ti (mol ratio) initial gel	Ce:Ti (mol ratio) final calcined
Ce−Ti (Meso), 673 K	357	3.6	0.63	1:1	nd
Ce−Ti (Meso), 773 K	349	3.6	0.61	1:1	0.8:1
Ce−Ti (Meso), 873 K	336	3.4	0.58	1:1	nd
Ce−Ti (Meso),1073 K	286	3.2	0.41	1:1	nd
Ce−Ti (Meso), 773 K	366	3.8	0.59	0.5:1	0.45:1
Ce−Ti (Meso), 773 K	351	3.4	0.55	1.5:1	1.4:1
Ce (Meso), 773 K	263	2.9	0.46		
Ti (Meso), 773 K	389	3.9	0.66		
Ce−Ti, 773 K	68				
Pt/Ce−Ti (Meso)	332	3.4	0.55		

III. Results and Discussion

Thermogravimetric analysis (TGA) of the as-made ceria−titania mesoporous material showed that organic template molecules could be completely removed by calcining the powders up to 673 K and that the weight loss between 673 and 1073 K was extremely small. From ICP analysis it was found that the Ce:Ti atomic ratios in the final calcined product was almost the same as the input Ce:Ti ratio during synthesis (Table 1). When the Ce/Ti ratio in the initial synthesis mixture was 1/1 (confirmed by ICP analysis), the ratio in the final calcined product was 0.8/1. Similarly, when the Ce/Ti ratio in the initial synthesis mixture were 0.5/1 and 1.5/1, the actual ratio in the final calcined product was 0.45/1 and 1.4/1, respectively. This indicates that there is only a slight difference in the Ce/Ti ratio before and after hydrothermal crystallization. A slight decrease in Ce concentration in the calcined product is due to washing out of some ceria component as observed by ICP analysis of the filtrate. The surface Ce/Ti ratio measured by XPS analysis was also the same as the bulk ratio.

Figure 1 shows typical X-ray diffraction (XRD) patterns for mesostructured ceria−titania (Ce/Ti = 1/1). A very broad XRD peak is observed at $2\theta = 1-3°$ typical for mesostructured materials (Figure 1i). All the other samples with different Ce/

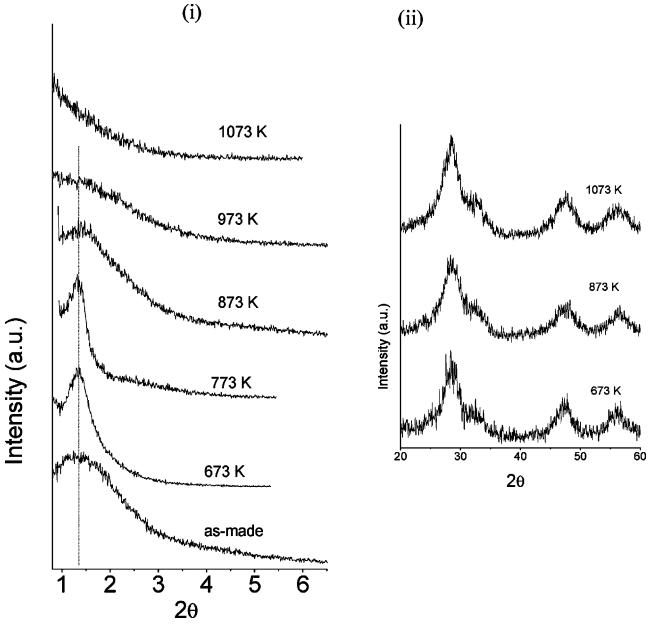

Figure 1. XRD pattern of mesoporous ceria−titania: (i) low-angle pattern; (ii) high-angle pattern.

Ti ratios (0.5/1, 1/1.5) also showed similar XRD patterns. It is observed that the broad peak in the 2θ range 1−3° in the as-made template containing ceria−titania sample becomes narrower and sharper after calcinations of the material up to 773 K. When the sample is further heated to 873 and 973 K, the low-angle XRD peaks shift slightly toward higher 2-theta value and there is a decrease in the peak intensities. This could be due to wall structuring during the template removal and higher temperature thermal treatment which is also accompanied by pore shrinkage. On further calcining the sample to 1073 K, the characteristic low-angle XRD peak due to framework-confined mesoporosity vanishes because of breakdown in the mesoporous structure.

Figure 1ii shows the wide-angle X-ray diffraction patterns of the CeO_2-TiO_2 sample calcined at different temperatures. All the diffraction peaks can be assigned to cubic, flourite CeO_2 (PDF−ICDD 34−0394), and no peaks because the TiO_2 phase could be observed indicating the absence of bulk titania phase (with crystallite size >3 nm) in these mesoporous materials. Preuss and Gruehn have reported various Ce−Ti−O oxides, namely, Ce_2TiO_5, $Ce_2Ti_2O_7$, and $Ce_4Ti_9O_{24}$, by heating appropriate mixture of solids containing Ce and Ti at 1523 K.[32] However, no such crystalline phases could be observed in the present study. The absence of crystalline Ce−Ti−O phases may be due to the differences in the preparation methods and lower calcinations temperatures employed in the present investigation. With increasing calcination temperature, a little peak narrowing and an increase in the intensity of the lines because of cubic CeO_2 can be observed. This implies that there is little sintering and agglomeration of ceria crystallites with increasing temperature, which is probably due to the effect of dispersed titania phase which inhibits the agglomeration of ceria phase. Also, there was no observable change in the ceria particle size in the mesoporous mixed oxides with different Ce/Ti compositions. In CeO_2-TiO_2 mixed oxides prepared by coprecipitation method, the presence of anatase titania phase along with cubic ceria phase has been invariably observed[33] by XRD, but in the present mesoporous CeO_2-TiO_2 materials, we do not observe any bulk titania phase; this could be due to very fine dispersion of titania nanocrystallites resulting from Ce−O−Ti type bonds.

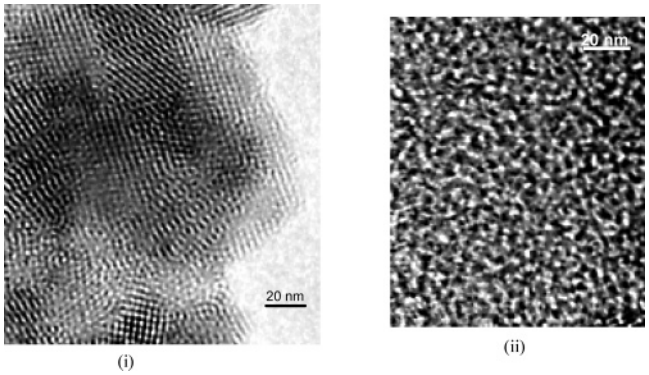

Figure 2. TEM image of mesoporous oxides (i) ceria−titania (773 K), (ii) ceria−titania (973 K).

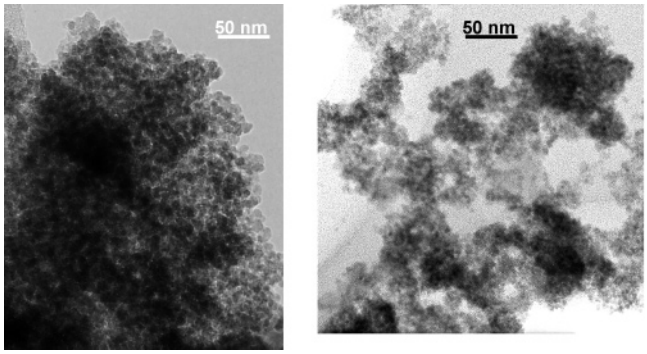

Figure 3. TEM image of mesoporous oxides ceria−titania (1073 K).

Such a fine dispersion of Ti in ceria matrix prevents the aggregation of titania even after heating the sample up to 1073 K. The *a* cell-parameter values for the CeO_2 (111) base peak[28] were calculated using the cubic indexing method. The *a* cell-parameter value for the calcined sample was 0.536 nm which was smaller than the 0.540-nm value for the pure CeO_2 phase which indicates that Ti^{4+} cation could enter the ceria lattice, resulting in the formation of solid solutions because the Ti^{4+} ionic radius (0.064 nm) is smaller than that of Ce^{4+} (0.097 nm).

The XRD results were verified by transmission electron microscopy, Figure 2. The micrograph displays a TEM of the calcined material. The presence of a disordered mesostructure is apparent. The observed disorder is consistent with the XRD of the mixed metal oxide, which shows the absence of additional indexable peaks in the pattern besides the broad d_{100} peak. The TEM of the sample heated to 973 K shows the presence of dense wormholelike mesopores resulting from the densification of the mesopore walls at higher temperatures and consequent pore shrinkage (as observed from pore size analysis). In the samples heated to 1073 K, the TEM does not show clearly the presence of disordered mesopores but a rather foamlike structure resulting from closely aggregated metal oxide nanoparticles is observed (Figure 3). The aggregation resembles aerogel materials such as titania−silica prepared by sol−gel method.[34]

The porous properties of calcined mesoporous ceria−titania and other reference materials are shown in Table 1. The N_2 adsorption−desorption isotherm for mesoporous ceria−titania is presented in Figure 4. The sample exhibits isotherm of type IV, typical of mesoporous materials with a well-defined step in the adsorption curve between partial pressures P/P_o of 0.4−0.8, and a large hysteresis loop due to capillary condensation in the mesoporous channels or cages. Barret−Joyner−Halenda (BJH) analysis of adsorption isotherm shows that the mesoporous ceria−titania mixed oxide (Ce/Ti = 1/1) calcined at 773

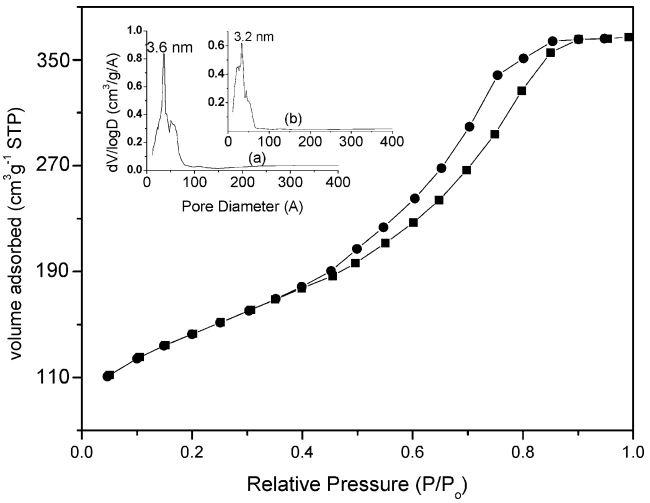

Figure 4. N_2 sorption analysis of mesoporous ceria−titania (773 K) (inset pore size distribution (a) 773 K (b) 1073 K).

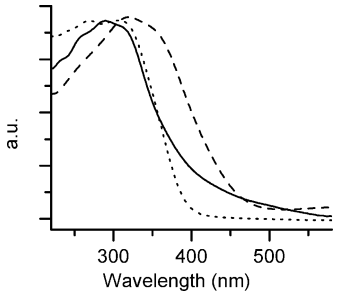

Figure 5. UV−vis diffuse reflectance spectra (DRS) of mesoporous samples: titania (dot), ceria (dash), and ceria−titania (line).

K exhibits a broad pore-size distribution with a mean pore size of 3.6 nm. The sample calcined at 1073 K shows smaller average pore size of 3.2 nm but the pore size distribution is broad even though the XRD analysis of the sample did not show any observable peaks in the low 2-theta range which indicates that the sample still retains the mesoporous structure but the local organization of pores is lost at 1073 K.

UV−vis diffuse reflectance spectra (DRS) of the mesoporous samples are plotted in Figure 5. Although the mesoporous CeO_2 sample presents its absorption edge at ca. 370 nm, the spectrum of mesoporous ceria−titania (Ce/Ti = 1/1) shows that ceria incorporation to TiO_2 induces a small red-shift of the electronic absorption with respect to the pure titania and significant blue-shift with respect to pure ceria. Previous studies on supported ceria samples have shown an increasing blue shift of the absorption edge of this material with decreasing the ceria loading and, consequently, the ceria average particle size.[35−37] This fact has been proposed to arise as a consequence of either the quantum size effect originated by the diminution of ceria particle size or the existence of larger contribution of $Ce^{4+}-O^{2-}$ charge-transfer transitions, which yield a relatively broad band with a maximum at ca. 280 nm.[35] Accordingly, small ceria particles, or highly dispersed cerium entities (either isolated or forming two-dimensional ceria patches on the support surface), display a larger intensity of the charge-transfer transition than the corresponding bulk oxide.[35,36] On this basis, the modification of the spectrum of mesoporous ceria−titania with respect to ceria is consistent with the presence of a dispersed ceria component.

TABLE 2: XPS Core-Level Binding Energies (eV) of CeO_2-TiO_2 Sample Calcined at Different Temperatures

	O(1s), eV			
material	$O_{lattice}$	OH^{-1}	Ti($2p_{3/2}$), eV	Ce ($3d_{5/2}$), eV
CeO_2-TiO_2 (873 K)	529.1	531.7	458.0	882.0
CeO_2-TiO_2 (1073 K)	529.2	531.7	458.2	882.0

The nature of interactions in the samples of CeO_2-TiO_2 (Ce/Ti = 1/1) calcined at different temperatures has been investigated by XPS technique. The electron-binding energies (eV) of the photoelectron peaks pertaining to O 1s, Ti 2p, and Ce 3d are shown in Table 2 and agree well with the values reported in the literature.[30,31,37] The representative photoelectron peaks of O 1s, Ti 2p, and Ce 3d pertaining to the mesoporous CeO_2-TiO_2 samples are depicted in Figures 6, 7, and 8, respectively. Figure 6 displays the O 1s XP spectra of CeO_2-TiO_2 samples calcined at different temperatures. As shown in Figure 6, the O 1s peak is, in general, broad and complicated because of the nonequivalence of surface oxygen ions. The peak shape suggests that it is composed of more than one peak arising from the overlapping contribution of oxygen from ceria, titania, and Ce−Ti−O compounds. The binding energy of the most intense O 1s peak slightly increased for the 1073 K calcined sample. The Ti 2p photoemission spectra of the sample exhibited typical XPS peaks around 458 eV for Ti $2p_{3/2}$ and at around 464 eV for Ti $2p_{1/2}$ (Figure 7). The peak separation between Ti($2p_{1/2}$) and Ti($2p_{3/2}$) signals is 5.8 eV, which is in agreement with the reported literature value.[38] The intensity of the Ti 2p core-level spectra increased with increasing calcination temperature probably because of better crystallization of TiO_2 because of elimination of residual carbon during calcination of samples in air at higher temperatures.

The Ce 3d XP spectra of mesoporous CeO_2-TiO_2 samples calcined at different temperatures are shown in Figure 8. The XPS core-level spectra of Ce 3d are generally characterized by complex but distinct features that are related to the final-state occupation of the Ce 4f level.[39] On the basis of the works of Burroughs et al.,[40] Pfau and Schierbaum,[37] and Creaser et al.,[41]

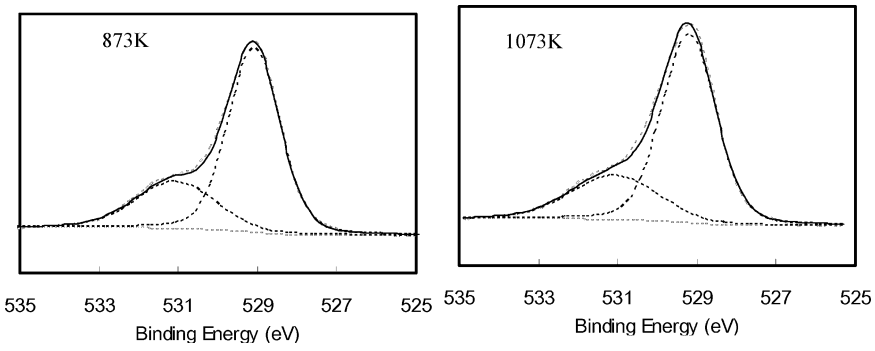

Figure 6. O 1s XPS spectra of mesoporous ceria−titania calcined at different temperatures.

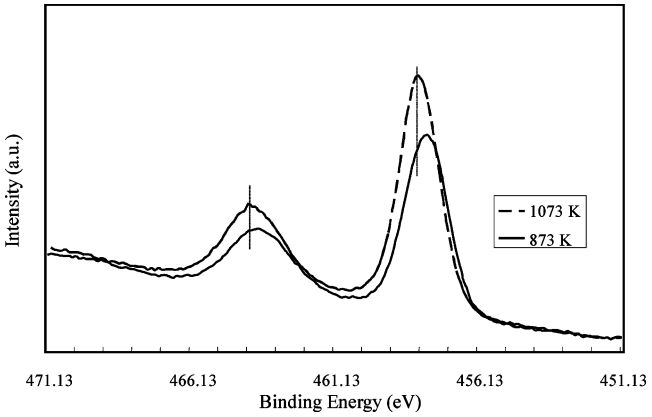

Figure 7. Ti 2p XPS spectra of mesoporous ceria−titania calcined at different temperatures.

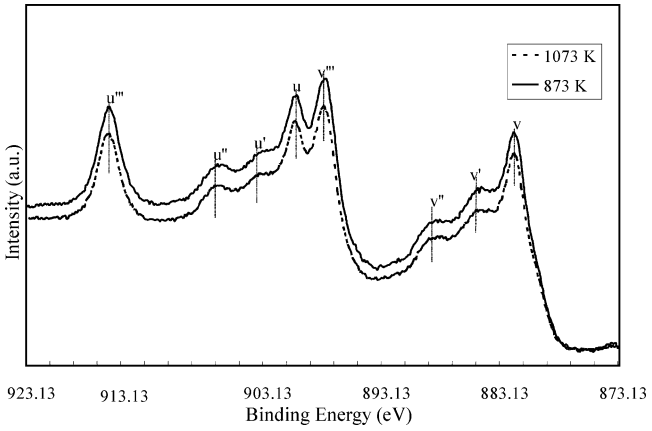

Figure 8. Ce 3d XPS spectra of mesoporous ceria−titania calcined at different temperatures.

the Ce 3d spectrum can be assigned as follows: The peaks labeled u are due to $3d_{3/2}$ spin−orbit states, and those labeled v are the corresponding $3d_{5/2}$ states. The u‴/v‴ doublet is due to the primary photoemission from Ce(IV)O_2. The u/v and u″/v″ doublets are shakedown features resulting from the transfer of one or two electrons from a filled O 2p orbital to an empty Ce 4f orbital. The u′/v′ doublet is due to photoemission from Ce (III) cations. The Ce 3d spectrum of the CeO_2-TiO_2 sample basically denotes a mixture of Ce^{3+}/Ce^{4+} oxidation states giving rise to a myriad of peaks indicating that the surface of the sample is not fully oxidized. With increasing calcination temperature, the intensity of the u′/v′ doublet due to primary photoemission from Ce^{3+} relative to the intensities of the peaks due to photoemission from Ce^{4+} (u‴/v‴) did not show any clear change. The presence of u′/v′ doublet peaks in the spectrum indicates that the CeO_2-TiO_2 sample contains some oxygen vacancies and is in a partially reduced state. Partial photoreduction of CeO_2 during XPS measurements is a well-known fact in the literature.[42−44] The reduction is mainly due to the progressive elimination of surface hydroxyls and oxygen ions from the CeO_2 surface upon vacuum treatment.

Figure 9 shows the results for the removal of toluene as representative volatile organic compound (VOC) after 24 h over the ceria−titania materials (with Ce/Ti = 1/1) calcined at 773 K which showed best performance among ceria−titania materials with different Ce/Ti ratios. The material showed considerable toluene removal ability at room temperature (about 30%) along with 19 ppm CO_2 formation indicating 3.4% partial oxidation/degradation of the toluene. When the same reaction was carried

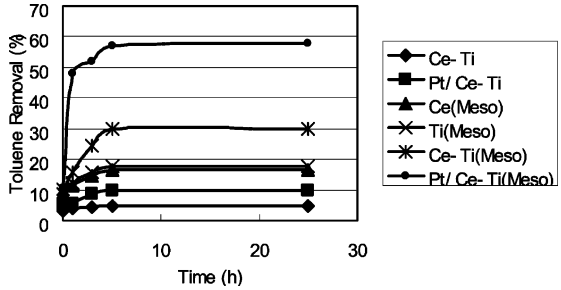

Figure 9. Toluene removal ability of mesoporous ceria−titania (Ce−Ti(Meso)), mesoporous ceria (Ce(Meso)), mesoporous titania (Ti(meso)), nonporous ceria−titania (Ce−Ti), and Pt impregnated mesoporous ceria−titania (Pt/Ce−Ti(Meso)) samples.

under daylight, there was no change in overall toluene removal but the CO_2 formation nearly doubled indicating photocatalytic decomposition of adsorbed toluene with 7.1% conversion. The toluene removal ability increased with temperature and reached about 40% along with 35 ppm CO_2 formation at 85 °C (Figure 1S) indicating 6.3% partial oxidation/degradation of the toluene. The result indicates that these materials are promising for developing indoor air-purification materials. This could be attributed to the presence of labile oxygen vacancies and mobile bulk oxygen species, as also indicated by Ce 3d XPS analysis (vide supra).

In comparison, under similar conditions nonporous ceria−titania prepared by the coprecipitaion method[28] showed very low toluene removal ability (<5%) (Figure 9). The toluene removal performance per unit area was about 1.2 times higher at room temperature and about 1.3 times higher at 85 °C for mesoporous ceria−titania compared to nonporous ceria−titania. Mesoporous ceria and mesoporous titania samples also showed lower intrinsic toluene removal ability (per square meter surface area) than mixed mesoporouse ceria−titania and only about 3−5 ppm of CO_2 was observed (<1% toluene conversion), implying that there was little toluene decomposition over these materials at room temperature (Figure 9). Also, the mesoporous ceria and mesoporous titania samples showed decreasing toluene removal ability with increasing temperature (up to 85 °C) implying weak adsorption of toluene over these materials (Figure 1S).

The toluene removal ability further improved after Pt impregnation (about 58%) (Figure 9) and reached about 67% at 85 °C (Figure 1S). Noble metals such as Pt are efficient total oxidation catalysts for which reaction may start at temperature as low as room temperature.[45] So in Pt deposited mesoporous ceria−titania, there is a synergetic effect; the noble metal site is a highly efficient oxidation site for toluene while the metal oxide site acts not only as an oxidation site but also provides active oxygen species for reaction. Hence, the toluene removal ability almost doubled after Pt impregnation. The high surface area ceria−titania mesoporous structure allows efficient Pt dispersion (83% from H_2 chemisorption) but the Pt dispersion was very low (24%) in nonporous ceria−titania material. The HRTEM image of Figure 10 reveals the shape and size distribution of the Pt nanoparticles on mesoporous ceria−titania surface. Analysis of 100 randomly selected particles indicates that the average diameters for the Pt nanoparticles are 2−5 nm. It is likely that most of the Pt nanoparticles are dispersed on the outer surface of the mesoporous mixed oxide, but the presence of smaller nanoparticles inside the 3.6-nm mesopores cannot be ruled out.

We could completely decompose the adsorbed toluene from the surface of the catalyst by thermal treatment at around 450

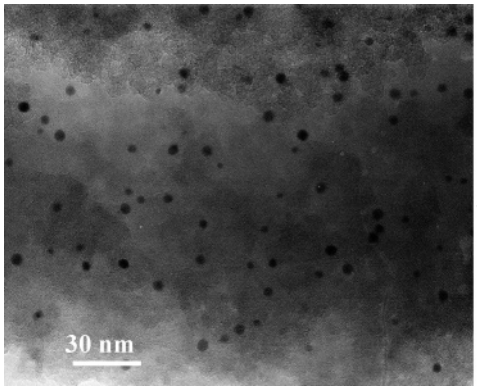

Figure 10. HRTEM image of the Pt nanoparticles on mesoporous ceria−titania surface.

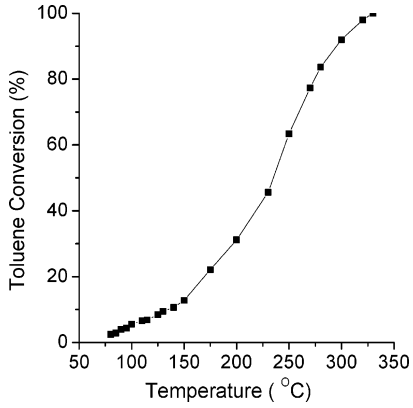

Figure 11. Activity of mesoporous ceria−titania in the total oxidation of 100 ppm toluene in air at 30 000 h^{-1} GHSV.

°C and the regenerated catalyst could be reused without any loss in activity. There was about 5% decrease in the removal performance after the catalyst was reused for six cycles. When the toluene combustion reaction was evaluated in a flow reactor, the toluene decomposition started well below 100 °C and it was possible to reach 100% toluene combustion at a temperature of 330 °C (Figure 11), whereas in nonporous ceria−titania the toluene combustion started well above 100 °C and total toluene combustion could be achieved only at 370 °C.

IV. Conclusions

In conclusion, we have successfully prepared thermally stable mesoporous ceria−titania mixed oxide. The material had high surface areas with a narrow pore size distribution in the mesoporous range after calcination up to 973 K. UV−vis and XPS analysis indicated the presence of well-dispersed ceria and titania components with negligible bulk oxide formation. The material showed high VOC (toluene) removal ability at room temperature compared to nonporous ceria−titania, mesoporous ceria, and mesoporous titania. The toluene removal ability almost doubled after Pt impregnation on mesoporous ceria−titania, most likely because of the synergetic effect between the Pt sites and the metal oxide sites. These results suggest that mesoporous ceria−titania mixed oxides are very promising for air-purification applications.

Acknowledgment. We would like to thank Mr. N. Suzuki, Ms N. Takahashi, and Mr. Y. Kawai of Toyota CRDL Inc. for TEM, XPS, and ICP analyses, respectively.

Supporting Information Available: Figure 1S temperature effect on toluene removal performance of mesoporous ceria−titania (Ce−Ti(meso)), mesoporous ceria (Ce(meso)), mesoporous titania (Ti(meso)), non-porous ceria−titania (Ce−Ti) and Pt impregnated mesoporous ceria-titania (Pt/Ce−Ti(meso)) samples. This material is available free of charge via the Internet at http://pubs.acs.org.

References and Notes

(1) Trovarelli, A. *Catal. Rev.—Sci. Eng.* **1996**, *38*, 439 and references therein.
(2) Nunan, J. G.; Robota, H. J.; Cohn, M. J.; Bradley, S. A. *J. Catal.* **1992**, *133*, 309.
(3) Serre, C.; Garin, F.; Belot, G.; Marie, G. *J. Catal.* **1993**, *141*, 9.
(4) Monteiro, R. S.; Dieguez, L. C.; Schmal, M. *Catal. Today* **2001**, *65*, 77.
(5) Imamura, S.; Fakuda, I.; Ishida, S. *Ind. Eng. Chem. Res.* **1988**, *27*, 718.
(6) Mishra, V. S.; Mahajani, V. V.; Joshi, J. B. *Ind. Eng. Chem. Res.* **1995**, *34*, 2.
(7) Trovarelli, A.; Dolcetti, G.; de Leitenburg, C.; Kaspar, J.; Finetti, P.; Santoni, A. *J. Chem. Soc., Faraday Trans. 1* **1992**, *88*, 1311.
(8) Zwinkels, M. F. M.; Jaras, S. G.; Menon, P. G. *Catal. Rev.—Sci. Eng.* **1993**, *35*, 319.
(9) Paparazzo, E. *Surf. Sci. Lett.* **1990**, *234*, L253.
(10) Mackrodt, W. C.; Fowles, M.; Morris, M. A. European Patent 91, 307,165, 1991.
(11) Laachir, A.; Perrichon, V.; Badri, A.; Lamotte, J.; Catherine, E.; Lavalley, J. C.; El Fallah, J.; Hilarie, L.; Leonormand, F.; Quemere, E.; Sauvion, G. N.; Touret, O. *J. Chem. Soc., Faraday Trans. 1* **1991**, *87*, 1601.
(12) Kubsh, J. E.; Rieck, J. S.; Spencer, N. D. *Stud. Surf. Sci. Catal.* **1994**, *71*, 109.
(13) Sauvion, G. N.; Caillod, J.; Gourlaouen, C. European Patent 0207,857, 1986.
(14) Ohata, T.; Tsuchitani, K.; Kitayuchi, S.; Nippon, S. K. Japanese Patent 8,890,311, 1988.
(15) Ashley, N. E.; Rieck, J. S.; Grace, W. R. U.S. Patent 484,727, 1991.
(16) Cho, B. K. *J. Catal.* **1991**, *131*, 74.
(17) Connell, M. O.; Morris, M. A. *Catal. Today* **2000**, *59*, 387.
(18) Rynkowski, J.; Farbotko, J.; Touroude, R.; Hilaire, L. *Appl. Catal., A* **2000**, *203*, 335.
(19) Pijolat, M.; Prin, M.; Soustelle, M.; Tourer, O.; Nortier, P. *J. Chem. Soc., Faraday Trans.* **1995**, *91*, 3941.
(20) Fallah, J. E.; Hilaire, L.; Normand, F. Le *J. Electron Spectrosc. Relat. Phenom.* **1995**, *73*, 89.
(21) Sun, D. L.; Heusing, S.; Puetz, J.; Aegerter, M. A. *Solid State Ionics* **2003**, *165*, 181.
(22) Johnson, B. D. *Photonics Mini Magazine (Laurin Publishing), December* **2003**.
(23) Martinez-Arias, A.; Fernandez-Garcia, M.; Ballesteros, V.; Salamanca, L. N.; Contesa, J. C.; Otero, C.; Soria, J. *Langmuir* **1999**, *15*, 4796.
(24) Crepaldi, E. L.; Soler-Illia, G. J. De A. A.; Bouchara, A.; Grosso, D.; Durand, D. *Angew. Chem., Int. Ed.* **2003**, *42*, 347. Corma, A.; Atienzar, P.; Garcia, H.; Chane-Ching, J. Y. *Nature Materials* **2004**, *3*, 394.
(25) Kresge, C. T.; Leonowicz, M. E.; Roth, W. J.; Vartuli, J. C.; Beck, J. S. *Nature* **1992**, *359*, 710.
(26) Sayari, A. *Microporous Mater.* **1997**, *12*, 149.
(27) Yang, D.; Zhao, D. Y.; Margolese, D. I.; Chmelka, B. F.; Stucky, G. D. *Nature* **1998**, *396*, 152. Zheng, J. Y.; Pang, J. B.; Qiu, K. Y.; Wei, Y. *Microporous Mesoporous Mater.* **2001**, *49*, 189.
(28) Reddy, B. M.; Khan, A.; Yamada, Y.; Kobayashi, T.; Loridant, S.; Volta, J. C. *J. Phys. Chem. B* **2003**, *107*, 5162.
(29) Goguet, A.; Meunier, F.; Breen, J. P.; Burch, R.; Petch, M. I.; Faur Ghenciu, A. *J. Catal.* **2004**, *226*, 382.
(30) *Practical Surface Analysis*, 2nd ed.; Briggs, D., Seah, M. P., Eds.; Auger and X-ray Photoelectron Spectroscopy; Wiley: New York, 1990; Vol. 1.
(31) Wagner, C. D.; Riggs, W. M.; Davis, L. E.; Moulder, J. F. In *Handbook of X-ray Photoelectron Spectroscopy*; Muilenberg, G. E., Ed.; Perkin-Elmer Corporation: Eden Prairie, MN, 1978.
(32) Preuss, A.; Gruehn, R. *J. Solid State Chem.* **1994**, *110*, 363.
(33) Coles, M. P.; Lugmair, C. G.; Terry, K. W.; Tilley, T. D. *Chem. Mater.* **2000**, *12*, 122.
(34) Bensalem, A.; Muller, J. C.; Bozon-Verduraz, F. *J. Chem. Soc., Faraday Trans.* **1992**, *153*, 88.
(35) Bensalem, A.; Bozon-Verduraz, F.; Delamar, M.; Bugli, G. *Appl. Catal., A* **1995**, *81*, 121.

(36) Martínez-Arias, A.; Fernández-García, M.; Salamanca, L. N.; Valenzuela, R. X.; Conesa, J. C.; Soria, J. *J. Phys. Chem. B* **2000**, *104*, 4035.
(37) Pfau, A.; Schierbaum, K. D. *Surf. Sci.* **1994**, *321*, 71.
(38) Sodhi, R. N. S.; Weninger, A.; Davies, J. E.; Sreenivas, K. *J. Vac. Sci. Technol.* **1991**, *A9*, 1329.
(39) Mullins, D. R.; Overbury, S. H.; Huntley, D. R. *Surf. Sci.* **1998**, *409*, 307.
(40) Burroughs, A.; Hamnett, A.; Orchard, A. F.; Thornton, G. *J. Chem. Soc., Dalton Trans.* **1976**, *1*, 1686.
(41) Creaser, D. A.; Harrison, P. G.; Morris, M. A.; Wolfindale, B. A. *Catal. Lett.* **1994**, *23*, 13.
(42) Paparazzo, E.; Ingo, G. M.; Zacchetti, N. *J. Vac. Sci. Technol., A* **1991**, *9*, 1416.
(43) Park, P. W.; Ledford, J. S. *Langmuir* **1996**, *12*, 1794.
(44) Fierro, J. L. G.; Soria, J.; Sanz, J.; Rojo, J. M. *J. Solid State Chem.* **1987**, *66*, 154.
(45) Pecchi, G.; Reyes, P.; Concha, I.; Fierro, J. L. G. *J. Catal.* **1998**, *179*, 309.